Nanoscale

PAPER

View Article Online
View Journal | View Issue

Cite this: *Nanoscale*, 2022, **14**, 5022

Photothermal nonlinearity in plasmon-assisted photocatalysis†

Ieng Wai Un, *[a] Yonatan Dubi [b] and Yonatan Sivan [a]

Received 27th November 2021,
Accepted 27th February 2022

DOI: 10.1039/d1nr07822d

rsc.li/nanoscale

Understanding the intricate relationship between illumination and temperature in metallic nano-particles is crucial for elucidating the role of illumination in various physical processes which rely on plasmonic enhancement but are also sensitive to temperature. Recent studies have shown that the temperature rise in optically thick ensembles of metal nanoparticles under intense illumination is dominated by the thermal conductivity of the host, rather than by the optical properties of the metal or the host. Here, we show that the temperature dependence of the thermal conductivity of the host dominates the nonlinear photothermal response of these systems. In particular, this dependence typically causes the temperature rise to become strongly sublinear, reaching even several tens of percent. We then show that this effect can explain experimental observations in several recent plasmon-assisted photocatalysis experiments. Under certain conditions, we show that thermal emission may also contribute to photothermal nonlinearity. This shows that any claim for the dominance of non-thermal electrons in plasmon-assisted photocatalysis must account first for this photothermal nonlinear mechanism.

1. Introduction

The use of illuminated metallic surfaces to enhance the yield of chemical reactions (aka plasmon-assisted photocatalysis) was proposed by Nitzan and Brus as early as 1981[1] and implemented experimentally shortly afterwards.[2] However, only after several decades of slow progress (see *e.g.*, ref. 3–8) has this line of research rapidly gained popularity following several high-impact publications (see, *e.g.* ref. 9–12 for some recent reviews). The growing interest was propelled by claims in some of the more famous papers on the topic[13–17] that the reaction rate increases due to the excitation of high-energy non-thermal electrons in the metal (aka "hot" electrons), which then tunnel out of the metal and provide the necessary energy for the reactants to allow them to be converted into the products more efficiently.

However, these very papers (ref. 13–17) were shown to suffer from technical and conceptual flaws (including improper temperature measurements, improper data normalization *etc.*; see discussion in ref. 18–22). Instead, a purely thermal mechanism was shown to be able to explain the experimental data quite convincingly.[18,20,22,23] In particular, a shifted Arrhenius Law for the reaction rate, $R \sim \exp\left(-\frac{\mathcal{E}_a}{k_B T(\mathbf{r}) + aI_{inc}}\right)$, whereby the temperature of the system was corrected for illumination-induced heating, was shown to provide an excellent fit to the published data, essentially with no fit parameters. This result was corroborated with the first ever complete calculation of the steady-state electron non-equilibrium in metals,[24] a consequent Fermi golden-rule argument[25] that pointed to the improbability of non-thermal electrons causing the catalysis, and detailed thermal simulations where the dynamics of the heat generated from each of the nanoparticles (NPs) in the system was properly modelled.[20] Similar criticism was raised in an independent study,[21] and a characterization that is in line with our approach was employed by several groups (see, *e.g.*, ref. 26–30).

In a subsequent paper,[31] it was shown that in many typical configurations, the tedious modelling of the contributions of each of the heated NPs in the sample can be replaced by an effective medium approximation. This approach also enables the exact reactor geometry, constituent materials and boundary conditions to be accounted for, thus enabling a quantitative comparison with the measured data (see Fig. 1(a)). This series of work was lately extended to also account for fluid dynamics effects and for redox reactions[32] (Fig. 1(b)).

The bottom line of thermal modelling is that when attempting to quantitatively separate thermal and non-thermal effects in plasmon-assisted photocatalysis experiments, one has to overcome a conceptual difficulty – the thermocatalysis control experiments must reproduce the *exact spatially non-uniform temperature profile* induced by the illumination, otherwise,

[a]*School of Electrical and Computer Engineering, Ben-Gurion University of the Negev, Beer-Sheva, 8410501, Israel. E-mail: iengwai@post.bgu.ac.il*
[b]*Department of Chemistry, Ben-Gurion University of the Negev, Beer-Sheva, 8410501, Israel*

†Electronic supplementary information (ESI) available. See DOI: 10.1039/d1nr07822d

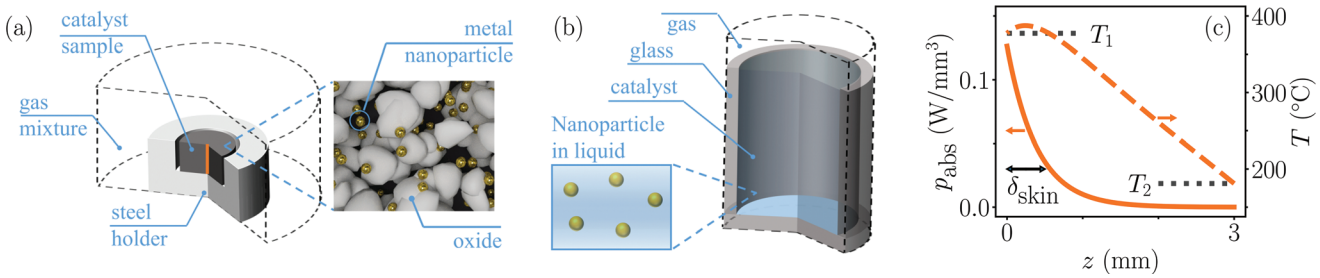

Fig. 1 (a) A schematic illustration of a photocatalytic chamber (left) and of a pellet-based catalyst sample (right). Note the sparsity of the metal nanoparticles and the near-percolation nature of the micron-size oxide particles. (b) A schematic illustration of a typical plasmon-assisted photocatalysis setup based on metal nanoparticle liquid suspension. In both set-ups, a heat flux boundary condition is applied to all domain boundaries (marked by dashed lines). (c) The heat source density (orange solid line) and temperature (orange dashed line) along the optical axis into the catalyst sample (labeled by the orange solid line in (a)). The black dotted lines represent the top (T_1) and the bottom (T_2) surface temperature.

when subtracting the thermocatalysis rate from the photocatalysis rate (*e.g.*, as in ref. 17 and 33), any difference between the temperature distributions in an inaccurate control and the corresponding photocatalysis experiment is bound to be incorrectly interpreted as "hot" electron action. This issue is particularly important because the Arrhenius Law shows that the reaction rate has an exponential sensitivity to the temperature distribution.[20]

Detailed measurements and/or calculations of the temperature distribution in the studied samples have indeed constituted a central role in several recent demonstrations of non-thermal effects in plasmon-assisted photocatalysis.[26–28,33,34] However, while the simple thermal calculations done so far were sufficient for relatively simple scenarios, they may not be sufficient to account for more complicated ones. These include, in particular, high-intensity illumination, which invokes steady-state nonlinear thermo-optic and photothermal effects,[35–39] which are usually simply ignored (without any justification). In the context of thin metal layers[40–43] and single NPs,[36–39,44,45] this effect has already been shown to cause deviations of several tens to hundreds of percent in the permittivity, and hence in the field and temperature distributions compared with the purely uniform linear thermal response. Note that such a nonlinear effect is far greater than conventional nonlinear optical effects.

In this work, we go beyond the study of the linear response and evaluate the importance of nonlinear photothermal effects in large random ensembles of metal NPs, suitable for plasmon-assisted photocatalysis experiments (Fig. 1(a) and (b)), but also for many other types of experiments in nonlinear optics (see *e.g.*, ref. 35 and 46–50). First, in section 2 we provide a qualitative analysis that points to the most important parameter that affects the overall nonlinear photothermal response of typical plasmon-assisted photocatalysis systems, namely, the (effective) thermal conductivity of the host. We also identify those parameters which have a negligible effect on the nonlinearity, namely, the optical parameters. Then, in section 3 we switch to a rigorous analysis and describe the methodology we employ to calculate the temperature distribution in the samples considered. The qualitative analysis is then applied in section 4 to two sets of experimental data taken from recent high-impact plasmon-assisted photocatalysis experiments. The good match of our analysis with the experimental data indicates that the photothermal nonlinearity is indeed a significant effect, such that neglecting to account for it is bound to lead to an overestimate of the role of non-thermal electrons. In section 5 we evaluate the contribution of thermal emission to the temperature rise and overall photothermal nonlinear response. We show that it gives rise to a significant contribution only for very high temperatures and/or systems characterized by a high emissivity. Section 6 provides a discussion and outlook.

2. A qualitative analysis

In order to achieve a qualitative understanding of the high-temperature and/or -intensity response of plasmon-assisted photocatalysis systems (*i.e.*, the photothermal nonlinearity), we start by considering a simplified configuration, namely, we assume that the sample consists of metal NPs (with dielectric permittivity $\varepsilon_m = \varepsilon'_m + i\varepsilon''_m$, thermal conductivity κ_m and NP number density n_p) distributed in a cylinder-shaped volume and immersed in a uniform host material (with thermal conductivity κ_h).

In our previous work,[31] we have shown that in the weak illumination limit, the temperature rise at the top center of such a sample can be approximately written as

$$\Delta T^{top} \approx \frac{I_{inc}\rho_b}{2\kappa_h}\left(1 - e^{-H/\delta_{skin}}\right), \quad (1)$$

where ρ_b is the beam radius, H is the sample thickness, and δ_{skin} is the penetration (skin) depth of light in the catalyst sample. The inverse of the penetration (skin) depth (*i.e.*, the absorption coefficient) is related to the NP number density n_p and the absorption cross-section σ_{abs} *via*

$$1/\delta_{skin}(\omega) = n_p\sigma_{abs}(\omega). \quad (2)$$

We now recall that in plasmon-assisted photocatalysis experiments, the light penetration depth is usually designed to be smaller than the sample thickness (*i.e.*, such that $H \ll$

$\delta_{skin}(\omega)$ for all wavelengths in the illumination) to ensure that all the illumination energy is absorbed; see Fig. 1(c). Eqn (1) shows that under such conditions, the temperature rise simply becomes $\Delta T^{top} \approx \frac{I_{inc}\rho_b}{2\kappa_h}$, so that the overall temperature rise is weakly sensitive to the illumination spectrum, NP shape, size and density, but exhibits an inverse relationship to the host thermal conductivity.[31] Many of these observations were verified experimentally in ref. 51.

When the illumination intensity is increased, the illumination-induced heating of the NPs causes a modification of the optical and thermal properties of the NPs and their surroundings. This effect gives rise to a nonlinear dependence of the sample temperature on the illumination intensity. Eqn (1) and its approximation shows that the photothermal nonlinearity would be dominated by the temperature dependence of the thermal conductivity of the host, κ_h. To understand this potentially non-intuitive result, we note that the increase in the imaginary part of the metal permittivity (ε''_m) with temperature reduces the quality factor of the plasmonic resonance of the NPs.[37–39] Meanwhile, the change in the real part of the metal permittivity (ε'_m) causes a resonance shift of the absorption spectrum. Although the impact of the change in the metal permittivity on the absorption cross-section varies in a complex manner with the NP size and the illumination wavelength (see *e.g.* ref. 37–39), and although the sensitivity of the metal permittivity to the rising temperature is relatively high,[37,41–43,48,52,53] the metal permittivity makes a relatively small contribution to the overall photothermal response of the sample when the penetration depth is much smaller than the sample thickness, as shown in eqn (1), because the sample absorbs all light regardless of these changes. Moreover, since the temperature dependence of the optical properties of the host has a similar effect on the absorption cross-section to the real part of the metal permittivity[38,39] (*i.e.*, it causes a resonance shift), the nonlinear response due to the change in the host permittivity is also small.

On the other hand, the contribution of the thermal properties to the overall photothermal nonlinearity is significant; it naturally depends on the volume fraction of the various materials. Because the metal occupies a small fraction of the sample volume, one can appreciate that the change in the metal thermal properties hardly contributes to the nonlinear response of the sample. In contrast, eqn (1) shows that the thermal properties of the *host* matter much more (be it gas, liquid, a porous composite or even a (dielectric) solid). Clearly, an illumination-induced increase in the thermal conductivity with the temperature means that the overall temperature rise in the sample will become sublinear as a function of the illumination intensity. Judging by the typical thermoderivative of these properties, the nonlinearity is expected to manifest itself at a temperature rise of several hundreds of degrees (see ref. 38 and 39); this estimate is found below to be in good agreement with the experimental data. Finally, in addition to the above, for very high temperatures and/or systems having high emissivity, the thermal emission will cause a further decrease in the temperature rise, resulting in an even stronger photothermal nonlinearity.[51]

3. Rigorous analysis

Now, having understood the expected qualitative behavior of the photothermal nonlinearity in plasmon-assisted photocatalysis, we turn to describing the methodology employed to study it rigorously. In order to properly account for the non-trivial reactor geometry and the multitude of materials, we used a numerical software package (COMSOL Multiphysics) to solve the time-independent heat (or Poisson) equation with temperature-dependent parameters.

Two generic configurations were used in plasmon-assisted photocatalysis experiments. One is based on pellet geometries (Fig. 1(a)) and the other on NPs in a liquid suspension (Fig. 1(b)). In both cases, we distinguish between the thermal conductivities of the catalyst sample and that of its surrounding to account for the inhomogeneity of the thermal properties, namely, we solve

$$\begin{cases} \nabla\cdot\left[\kappa_{cata}(T(\mathbf{r}))\nabla T(\mathbf{r})\right] = -p_{abs}(\mathbf{r}), & \text{inside the catalyst,} \\ \nabla\cdot\left[\kappa_{holder}(T(\mathbf{r}))\nabla T(\mathbf{r})\right] = 0, & \text{in the sample holder,} \\ \nabla\cdot\left[\kappa_{gas}(T(\mathbf{r}))\nabla T(\mathbf{r})\right] = 0, & \text{elsewhere.} \end{cases} \quad (3)$$

Here, $\kappa_{cata}(T(\mathbf{r}))$, $\kappa_{holder}(T(\mathbf{r}))$ and $\kappa_{gas}(T(\mathbf{r}))$ are the temperature-dependent thermal conductivities of the catalyst,[20,31] sample holder and surrounding gas, respectively. Finally, p_{abs} is the heat source density induced by the light absorption in the random metal NP array; it is well described by the effective medium approximation for the electromagnetic properties of the catalyst sample.[31] When the skin (penetration) depth is much smaller than the sample thickness one can neglect the temperature variation within the skin depth, namely,

$$p_{abs}(\mathbf{r}) = \int \frac{i_{inc}(\rho,\omega)}{\delta_{skin}(\omega,T_1)}\exp\left(-\frac{z}{\delta_{skin}(\omega,T_1)}\right)d\omega. \quad (4)$$

Here, ρ is the distance from the propagation optical axis, z is the distance along the propagation direction of the incident beam from the top surface of the catalyst sample and $i_{inc}(\rho,\omega)$ describes the transverse spatial and spectral profile of the incident beam. T_1 represents the temperature of the top layer of the catalyst sample and is now an *unknown* variable that needs to be determined by solving eqn (3) and (4) self-consistently. In practice, in eqn (4) (specifically, when calculating the absorption cross-section), T_1 is chosen to be 300 K since the only available data for the metals used as catalysts in the papers we analyze below (Ru and Cu) are at 300 K. In fact, this is a very good approximation for eqn (4) because, as pointed out in section 2, the temperature dependence of the permittivities has a minor effect on the overall photothermal response when the skin (penetration) depth is much smaller than the sample thickness. In addition, this approximation also allows significant saving of time and computational resources. In contrast, when the skin depth is comparable with the sample thickness, one needs to account for the temperature dependence of the permittivities and the temperature variation within the skin depth (see ESI section S1† for a complete deri-

vation). In this case, the expression for the heat source density becomes much more complicated than eqn (3) (see eqn (S2)†) and one needs to solve eqn (3) with eqn (S2)† self-consistently. The earlier analysis of the temperature dependence of the permittivities[37–39] implies that even in this case one should expect a sublinear growth of the temperature.

In order to limit the simulation domain to a realistic and significant volume, we set a convection heat flux boundary condition at the outer surfaces of the simulation domain; this models the heat transfer driven by the temperature difference between the simulation domain and the distant surrounding (assumed to be at 20 °C). The associated heat transfer coefficient (denoted by h in COMSOL Multiphysics) is used as an adjustable parameter to fit the experimental results in the small intensity limit for which one can neglect the temperature dependence of the thermal conductivities. In this case, eqn (3) becomes a linear Poisson equation, the solution of which is the linear approximation of the solution of eqn (3). The obtained value for h has a negligible effect on the photothermal nonlinearity (see Fig. S5†). We emphasize that the frequently employed fixed temperature boundary condition does not represent correctly the heat transfer from the reactor to the environment. Instead, it effectively brings the distant cool regions closer to the reactor, and thus cools the reactor in a manner that is inconsistent with the measured experimental data.

For simplicity, we apply the non-convection approximation. This was justified by simplistic estimates[20] that showed that the standard gas flow level used is not expected to be significant in removing the generated heat and further supported by simulations of natural and forced convection done in ref. 32; this effect anyhow is not expected to affect the nonlinear response.

4. Analysis of experiments

In the following, we apply the model described above to two representative experiments. Both involve pellet geometries which are typically composed of a large number ($\sim 10^{12}$–10^{14}) of metal NPs of a few nm, randomly distributed within a highly sparse 3D powder of micron-size metal oxide particles (see Fig. 1(a)); gases occupy the volume between the NPs. In a typical reaction chamber, the catalyst sample (typically a few mm in size) is placed on a (stainless steel) sample holder and the reaction rate is then measured under a specific illumination and/or under resistive heating.

The heat conduction in such a catalyst sample might be expected to be dominated by the solids (the sample holder and the oxide) since their thermal conductivities are much larger than those of the gases. However, this is not the case and instead, as shown previously,[31] it is the thermal conductivity of the gases that dominates the heat conductance. To see that, we first note that since for all practically useful samples and in all the cases we study below, the heat generation occurs primarily on the top layer of the catalyst sample, *i.e.*, away from most of the sample holder, the sample holder is effective in reducing the bottom-surface temperature but is less effective in reducing the top-surface temperature (see ESI section S3.2† for details).

Second, in such samples, the oxide fill factor typically only reaches ~10% (see eqn (S5)†). Indeed, the sample consists of a highly sparse random array of micron-sized oxide particles, which are barely touching each other (see Fig. 1(a)); thus, somewhat unintuitively the gas serves as the bottle-neck for the heat conduction in the catalyst sample and the heat conduction through the oxide is highly inefficient. This conceptual picture has been verified by a hierarchy of effective medium approaches that was found to be in good agreement with the experimental results (see ref. 54). Specifically, that work showed that the Maxwell–Garnett model[55,56] provides an excellent approximation for the effective thermal conductivity $\kappa_{\mathrm{cata}}^{\mathrm{eff}}$ of the catalyst sample we analyze below, namely (see ESI section S3.2† for details),

$$\kappa_{\mathrm{cata}}^{\mathrm{eff}} = \kappa_{\mathrm{gas}} + \frac{3 f_{\mathrm{oxide}} \kappa_{\mathrm{gas}}}{\dfrac{\kappa_{\mathrm{oxide}} + 2\kappa_{\mathrm{gas}}}{\kappa_{\mathrm{oxide}} - \kappa_{\mathrm{gas}}} - f_{\mathrm{oxide}}}, \tag{5}$$

where κ_{oxide} is the thermal conductivity of the oxide. Thus, since the fill factor of the oxide is small ($f_{\mathrm{oxide}} \ll 1$), the effective thermal conductivity of the catalyst sample becomes approximately $\kappa_{\mathrm{cata}}^{\mathrm{eff}} \approx (1 + 3 f_{\mathrm{oxide}}) \kappa_{\mathrm{gas}}$ (see eqn (S3)–(S6)†), *i.e.*, it is very close to that of the gas mixture and thus increases with temperature. This conclusion is validated by a recent experimental study of the temperature non-uniformities in plasmonic catalyst samples under illumination using fiber Bragg grating sensors; see Fig. S3.† Due to the above, in the examples below we set $\kappa_{\mathrm{cata}} = \kappa_{\mathrm{cata}}^{\mathrm{eff}}$.

4.1. Analysis of experiments from Li *et al.*, *Nano Lett.*, 2019, 19, 1706[57]

First, we look at the experimental results of Li *et al.*,[57] who studied ammonia synthesis using a cesium-promoted, magnesium-oxide supported, ruthenium (Ru–Cs/MgO) catalyst. The Ru NPs in this study were estimated to be ~2 nm in diameter. The catalyst sample (3 mm height and 6 mm diameter) was put in a reaction chamber equipped with a quartz window (which allows the catalyst sample to be illuminated at varied intensities and wavelengths) and a temperature controller (which is used to heat up the catalyst sample). The illumination spot was set to have the same size as the catalyst surface area. Two thin thermocouples were inserted into the catalyst sample, one to measure the top-surface temperature (denoted by T_1) and the other to measure the bottom-surface temperature (denoted by T_2). A mixture of N_2, H_2, and Ar with a ratio of 1 : 3 for N_2/H_2 flowed into the reactor at a total flow rate of 75 sccm. The gaseous product (NH_3) was monitored using an online mass spectrometer. For these parameters, an estimate similar to the one done in ref. 20 shows that the gas flow may affect the temperature by no more than 10%, justifying the use of the non-convection approximation in the following analysis.

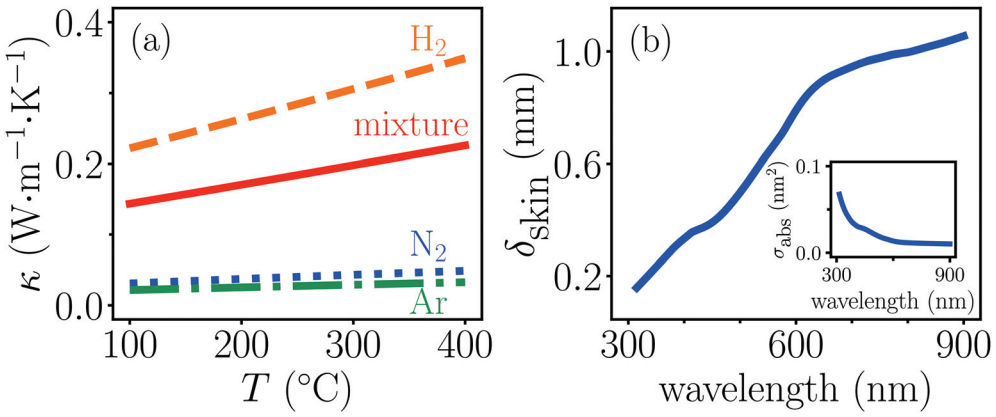

Fig. 2 (a) Temperature dependence of the thermal conductivities of N_2 [58] (blue dotted line), H_2 [59] (orange dashed line), argon[60] (green dash-dotted line) and the mixture used in ref. 57 (red solid line). (b) Light penetration (skin) depth and the absorption cross-section of the Ru NP (inset) as a function of the illumination wavelength.

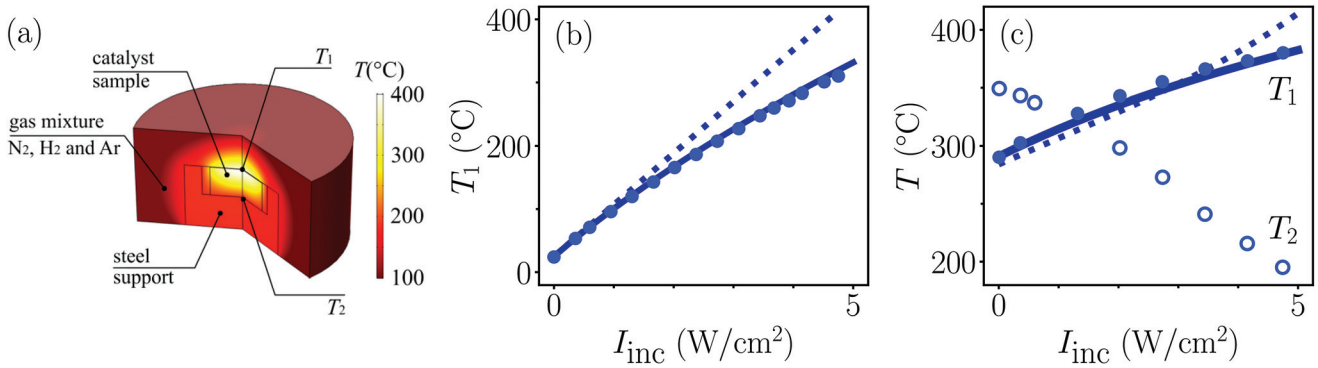

Fig. 3 (a) Details of the photocatalytic chamber and the temperature distribution at the illumination intensity I_{inc} = 5 W cm^{-2}. (b) T_1 (blue solid symbols, experimental data extracted from ref. 57; blue solid line, COMSOL simulation; blue dotted line, COMSOL simulation with the linear approximation) as a function of the illumination intensity for the blue light source without resistive heating. (c) Same as (b) but under resistive heating. The blue opened symbols represent the experimental data of T_2.

The temperature-dependent thermal conductivities of the input gases[58–60] are shown in Fig. 2(a). Since H_2 has a small molecular mass and a small molecule size, its thermal conductivity is much larger than those of N_2 and Ar. As a result, the thermal conductivity of the gas mixture is ~60% of the H_2 thermal conductivity. The thermal conductivity of the catalyst sample is related to the volume fraction of the oxide using the Maxwell Garnett equation[20,55,56] (see ESI section S2†).

The absorption cross-section of the Ru NPs and the light penetration depth in the sample are calculated using the permittivity of Ru at 300 K from ref. 61 and eqn (2); see Fig. 2(b). For wavelengths $300 < \lambda < 600$ nm, the penetration (skin) depth (eqn (2)) is $\delta_{skin} < 750$ μm, indeed much smaller than the sample thickness; thus, from ref. 31, we do not expect the numerical results to be sensitive to the exact parameters in this spectral regime. However, for $\lambda > 700$ nm, we find that $\delta_{skin} \gtrsim 1$ mm, so that here the penetration (skin) depth is only 2–3 times thinner than the sample thickness (see Fig. 2(b)); accordingly, one may expect a slight sensitivity to the various parameters in this regime. In addition, we assume that the transverse profile of the illumination intensity is uniform (denoted as I_{inc}).

To obtain the temperature distribution, we perform a full simulation including the catalyst sample, the sample holder and the reaction chamber with a few simplifications. Specifically, we simplify the complicated reaction chamber by assuming it has a cylindrical shape (1 cm height and 2 cm diameter) and that the catalyst sample (having the same size as used in the experiment) is placed in a steel holder; see Fig. 3(a).‡

In ref. 57, two experiments were performed. In the first, no resistance-heating was used; the simulation results of the top-surface temperature T_1 for $h \approx 70$ W m^{-2} K^{-1} demonstrate an excellent match to the experimental data; see Fig. 3(b) (the simulation result of the bottom-surface temperature T_2 is shown in Fig. S1(a)†). In order to demonstrate the actual level of

‡ The geometries of the reactor chamber, the sample holder and the catalyst sample were directly obtained from the authors of ref. 57 and 62.

the photothermal nonlinearity, we also performed a simulation under the linear approximation, namely, we neglected the temperature dependence of the thermal conductivity of the gas mixture. Fig. 3(b) shows that the linear approximation overestimates the nonlinear solution by more than 30% for a temperature rise of ~300 °C; this is an unusually large nonlinearity.

In the second experiment, the authors studied the effect of the temperature gradient on the reaction rate and the dependence of the temperature gradient on the illumination wavelength and intensity. To do that, they measured the intensity-dependent T_1, T_2 and reaction rate using four different light sources (UV, blue light, white light and NIR) and adjusted the resistive heating such that the equivalent temperature§ remained the same (325 °C) for all four light sources and all intensities.[57] Accordingly, we use the same simulation configuration to calculate the temperature distribution. Since the description of the resistive heating apparatus is not available in ref. 57, we simply set the temperature of the bottom of the catalyst sample to the reported T_2 as a constraint so as to mimic the resistive heating. The simulation results for the top-surface temperature T_1 again demonstrate an excellent match with the experimental data for blue, UV and white light sources,¶ see Fig. 3(c) and Fig. S1(b).† We find that the linear approximation deviates from the nonlinear solution by ~10% for a temperature rise of ~100 °C. For the NIR light source, the simulation results fit well with the experimental data; see Fig. S1(b).† As mentioned, in this case, the light-penetration depth is closer to the sample thickness (see Fig. 2(b)) so that the temperature distribution might become less insensitive to the change in permittivity of the Ru NPs with temperature. In that regard, the use of the Ru permittivity data at 300 K in the simulation is one possible reason for the small mismatch between the simulation results and the experimental data. Except for this minor discrepancy, the analysis here reinforces the conclusion of ref. 57 that the catalytic effect of the Ru–Cs/MgO system on the ammonia synthesis reaction is purely thermal.

An earlier work[62] by the same group employed a similar experimental system to study the carbon dioxide hydrogenation reaction using a titanium oxide-supported rhodium catalyst. Although the gas composition was different from that in ref. 57, the thermal conductivities of the gas mixtures[59,60,63] were similar since the gas mixtures had a similar fraction of H_2 in these two works. We simulated the temperature for the experiment without resistive heating at low temperatures (25 °C < T_1 < 120 °C) and found very good agreement with the experimental data (see ESI Fig. S6†). This explains the observed photothermal nonlinearity (~10%) for a similar temperature rise of ~100 °C (see Fig. S8 in ref. 62). However, a much larger nonlinearity was reported in the experiments with resistive heating at high temperatures (250 °C < T_1 < 450 °C); in fact, some of the data show an unusually large increase in T_1 for 300 °C $\lesssim T_1 \lesssim$ 375 °C and then a small growth rate in T_1 for $T_1 \gtrsim$ 375 °C. Accordingly, this cannot be explained by our (nonlinear) thermal model. Ruling out possible measurement artifacts in the data, it is natural to advocate for the possibility of non-thermal electrons contributing to the catalyzed reaction rate. However, a convincing interpretation of this experiment might require a dedicated explanation of the origin of the large nonlinearity.

4.2. Analysis of experiments from Zhou *et al.*, *Science*, 2018, 362, 69[17]

We now move on to show that the photothermal nonlinearity also explains the experimental measurements described in ref. 17. This work employed a similar setup to study ammonia decomposition on a MgO–Al_2O_3-supported Cu–Ru catalyst; however, unlike the papers studied in section 1, the nonlinearity is much stronger due to the higher temperature rises caused by the much smaller thermal conductivity of NH_3 [64,65] (see Fig. 4(a)), as well as the higher incident intensities used (see Fig. 4(c)). More importantly, while the authors of ref. 57 measured the sample temperature properly, significant concerns regarding the validity of the temperature measurements in ref. 17 have been raised (see discussion in ref. 18–20, 22 and 23). Therefore, in what follows, we rely only on a *calculation* of the temperature as well as on an extraction of it from the reaction rate using the Arrhenius equation. These approaches were shown to match well with the fitted temperatures; see ref. 18, 20 and 22.

We follow the procedure described in ref. 20 to extract the temperature out of the reaction rate. Specifically, we first obtain the activation energy 1.18 eV by fitting the experimental data in the dark (Fig. 1d in ref. 17) to an Arrhenius curve. Next, due to the failure to measure the light-induced temperature rise in ref. 17 (see ref. 18 and 19), we distinguish between the actual temperature of the reactor (denoted as $T(I_{inc})$) and the experimentally measured temperature (denoted as T_M; see Fig. S11D in ref. 17). The difference between $T(I_{inc})$ and T_M was found to be $T(I_{inc}) = T_M + \tilde{a}I_{inc} + \tilde{b}{I_{inc}}^2$, where I_{inc} is in W cm^{-2} and $T(I_{inc})$ and T_M are in K. The experimentally measured temperature T_M *vs.* I_{inc} is also fitted to a second-order polynomial, giving $T_M = 298 + 80I_{inc} - 3.8{I_{inc}}^2$. Then, we fit the measured reaction rate data under illumination (Fig. 1d in ref. 17) to a temperature-shifted Arrhenius curve,[20] *i.e.*, $R(I_{inc}) = R_0 \exp\left(-\frac{E_a}{k_B T(I_{inc})}\right)$, leading to $T(I_{inc}) = T_M + 180I_{inc} - 8{I_{inc}}^2$; see Fig. 4(c)–(e). This shows that the photothermal nonlinearity becomes nearly ~50% at the highest intensity used. This also shows that the temperature rise due to photon absorption becomes a sublinear function of the illumination intensity at high temperatures (as predicted in ref. 37–39 for a single metal nanoparticle) so that unlike the claims in ref. 66 (see p. 270 and on), the maximal temperature reached is

§ The equivalent temperature T_e is defined in ref. 57 and 62 through the relation $e^{-E_a/k_B T_e} = \frac{1}{T_2 - T_1}\int_{T_1}^{T_2} e^{-E_a/k_B T} dT$.

¶ The simulation results for UV and white light sources are shown in Fig. S1(b)† because they almost overlap with the results for the blue light source. This is a direct consequence of the weak sensitivity of the temperature distribution to the illumination wavelength when the penetration depth is much smaller than the sample thickness, conforming with the analysis in ref. 31 and experimental verification in ref. 51.

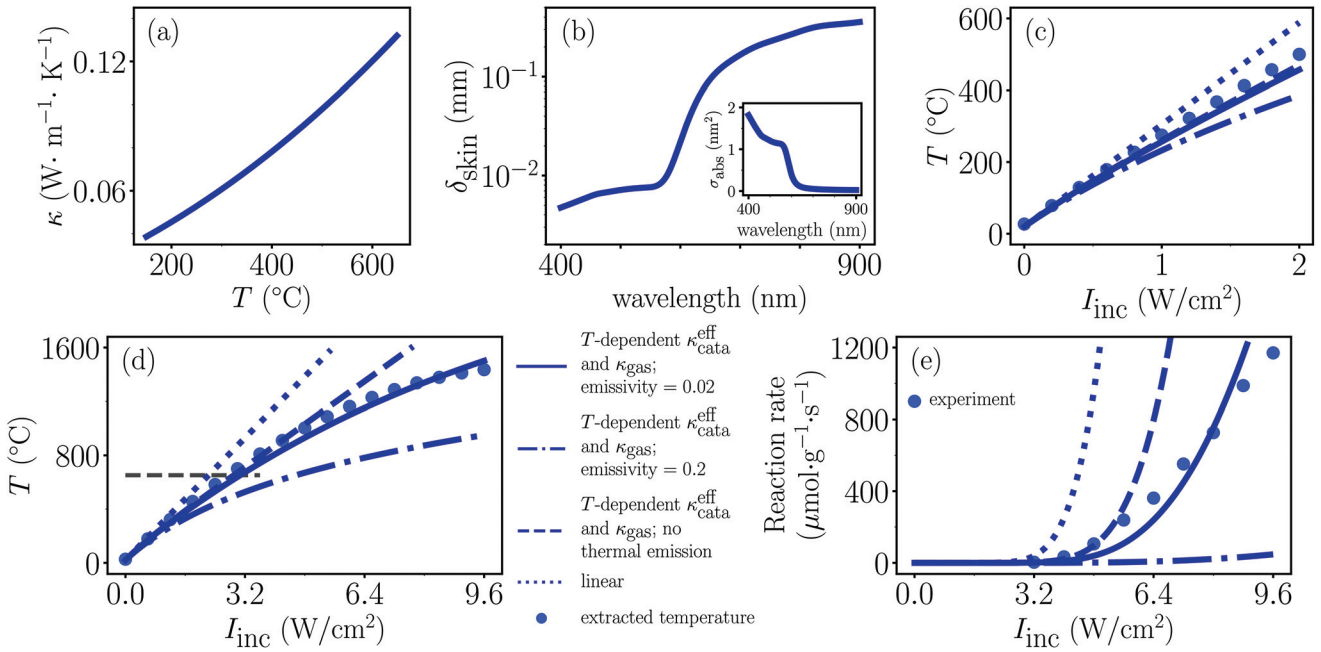

Fig. 4 (a) Temperature dependence of the thermal conductivity of NH_3.[64,65] (b) Light penetration depth and the absorption cross-section of the Cu–Ru NP (inset) as a function of the wavelength. (c) Simulation results of the temperature at the center of the top surface as a function of the illumination intensity (blue solid line (temperature-dependent thermal conductivities ($\kappa_{gas}(T)$ and $\kappa^{eff}_{cata}(T)$) and emissivity ε = 0.02) and blue dash-dotted line (temperature-dependent thermal conductivities ($\kappa_{gas}(T)$ and $\kappa^{eff}_{cata}(T)$) and emissivity ε = 0.2)) and its linear approximation (blue dotted line); the blue dashed line represents the simulation result without accounting for the thermal emission (temperature-dependent thermal conductivities ($\kappa_{gas}(T)$ and $\kappa^{eff}_{cata}(T)$) only). (d) An extension of (c) to the high illumination region. The black dashed line represents the upper bound of the temperature range of the NH_3 thermal conductivity measured in ref. 64. (e) Calculated reaction rates (the blue solid line, the blue dashed line and the blue dotted line) as a function of the illumination intensity. The blue circles in (c), (d) and (e) represent the numerical fit of the experimental data using the temperature-shifted Arrhenius law; see text for details.

~1400 °C rather than ~2700 °C. This result shows that claims that our thermal model predicts temperatures which are unrealistically high are incorrect.

The question remains – what is the reason for this massive sublinearity in the temperature-rise-*versus*-intensity relation? To answer this question, we adapt the simulation configuration used in section 1 to the experimental setup described in ref. 17 and simulate the temperature distribution *via* the heat transfer module of COMSOL Multiphysics. The thermal conductivity of NH_3 is taken from the experimental measurement of ref. 64 and 65 for the temperature range of 52–652 °C.‖ The measured data were also fitted in ref. 64 by the following cubic polynomial: $\kappa_{NH_3}(T) = 5.237 \times 10^{-4} + 5.179 \times 10^{-5}T + 8.404 \times 10^{-8}T^2 + 1.557 \times 10^{-11}T^3$, where κ_{NH_3} is in W m^{-1} K^{-1}) and T is in K, as shown in Fig. 4(a). This cubic polynomial is used in our simulations to extrapolate the NH_3 thermal conductivity for temperatures higher than 652 °C.

The catalyst sample was illuminated by a pulsed broadband white-light source (Fianium, WL-SC-400-8, 400–900 nm, pulse duration 4 ps, repetition rate 80 MHz, and a 2 mm diameter beam profile on the catalyst sample surface) without applying any resistive heating.[17] The penetration (skin) depth to the sample was calculated using the permittivity data of Cu and Ru at 300 K.[61] We found that the penetration depth was much smaller than the sample thickness; see Fig. 4(b). In addition to the temperature distribution, we also calculated the reaction rate based on the Arrhenius equation using the calculated temperature at the center of the top sample surface. For the above temperature range, our simulation results show satisfactory agreement with the fitted data, although they are independent of the fit procedure. In fact, the agreement extends up to 1000 °C, *i.e.*, even beyond the expected bound for the validity of the used values for the thermal conductivity of the host; see Fig. 4(c) and (d). In particular, the temperature at the center of the top surface increases monotonically with the illumination intensity but with a decreasing slope. In the original paper,[17] this sublinear growth of the temperature rise with the illumination intensity was *incorrectly* attributed to the temperature dependence of the thermal conductivity of the oxide support. This claim is, however, invalid for two reasons. First, this claim would lead to an opposite trend to that observed since the thermal conductivity of the MgO–Al_2O_3 support *decreases*

‖Although the thermal conductivity of NH_3 was measured at pressures of 12.9, 26.5, and 45.0 kN m^{-2} (0.127, 0.262 and 0.444 atm) in ref. 64, this data can be used for the simulation at 1 atm since the gas thermal conductivity is very weakly dependent on the pressure.[67] To justify this, we compared the data from ref. 64 with the data measured at 1 atm but in the lower temperature range (−33.6–426.9 °C) provided in ref. 65 and found good agreement between these two sets of data.

with temperature.[68] Second, the temperature dependence of the thermal conductivity of the oxide support, in fact, was shown in ref. 31 to have a negligible effect on the overall nonlinearity because of the small volume fraction of oxides in the catalyst sample (using the sample mass and the sample volume reported in ref. 17). Instead, in agreement with the qualitative analysis and the modelling of the papers studied in section 1, the sublinear growth of the temperature rise with the illumination intensity is mainly due to the increase in the gas thermal conductivity with temperature.[64,65]

One of the possible reasons for the discrepancy observed for $T > 1000$ °C between the simulation results and the fitted data at high intensities is the inaccuracy induced by the extrapolation to the thermal conductivity data of NH_3. This is because the third-order term (T^3) in the cubic polynomial used for the extrapolation has the same order of magnitude as the second-order term (T^2) for temperatures higher than 1000 °C, *i.e.*, it is likely that higher-order terms are required for better accuracy. Another possible but minor reason is the usage of the permittivity data at 300 K for Cu in the simulation.** However, since the light penetration depth is much smaller than the sample thickness, the change in the optical properties of Cu could only have a minor effect on the overall photothermal nonlinearity; see discussion in ref. 31. Since comprehensive data for the temperature dependence of the metal permittivity and of the gas thermal conductivity hardly exist in such high-temperature regimes, the resolution of this discrepancy requires further experimental study.

5. Contribution of thermal emission to the photothermal nonlinearity

Another possible reason, especially relevant for the highest temperature range, is thermal emission, which may have a significant effect on the photothermal nonlinearity for high temperatures. Indeed, at the high temperatures reached in the experiments discussed above, one may wonder whether thermal emission can contribute to the energy balance and, thus, affect the steady-state temperature. This was claimed in ref. 17, by equating the density of absorbed photon power to the power loss due to heat conduction and thermal emission (based on the Stefan–Boltzmann Law); this claim, however, was not supported by any quantitative argument (see section 2 for a discussion of other faulty claims in ref. 17 in this context). In fact, in ref. 19 the role of thermal emission was claimed to be negligible by some of the authors of the current work. However, the heat conduction in ref. 19 was overestimated, since it was associated with the scale of a single nanoparticle, whereas the thermal emission was associated with the macroscopic (sample-scale) temperature gradient.

In order to resolve this argument, in what follows we evaluate thermal emission in plasmon-assisted photocatalysis samples by adding to heat equations such as eqn (3) a term responsible for the energy loss *via* thermal emission (again, based on the Stefan–Boltzmann Law), and comparing the relative importance of heat conduction and radiation.

We first revisit the experiments analyzed above. In Li *et al.* (ref. 57), the temperatures were moderately high (<400 °C) and the emissivity ε of the MgO host was relatively low (~0.2–0.55[71]). Specifically, for the temperature rise of $\Delta T \sim 300$ °C at the illumination intensity of 5 W cm^{-2}, the thermal energy loss due to thermal emission was around $\varepsilon\sigma((T_0 + \Delta T)^4 - T_0^4) \sim 0.03I_{inc} - 0.08I_{inc}$ where $\sigma = 5.67 \times 10^{-8}$ W m^{-2} K^{-4} is the Stefan–Boltzmann constant. Accordingly, we conclude that the thermal emission in this experiment is negligible. Similar results were found for Zhou *et al.*,[17] even up to ~1000 K. However, in the range of the highest intensities used in this work, the temperatures were even higher so that there might have been a significant contribution of thermal emission. As shown in Fig. 4(d) and (e), one can obtain a better match between the model and the numerical fit using the temperature-shift Arrhenius Law if the emissivity is set to 0.02, as estimated in ref. 18. If the emissivity is set to be 0.2, the photothermal nonlinearity becomes even stronger but shows a large mismatch with the extracted temperature and the experimental data. This indicates that, on the one hand, further experimental study of the emissivity of the catalyst sample at high temperatures is required, while on the other hand accounting for the thermal emission properly requires a more comprehensive model.

In contrast to these experiments which were characterized by low-emissivity samples, a recent experimental work[51] employed a high-emissivity sample. In particular, the sample in ref. 51 consisted mostly of high-emissivity alumina (in contrast to ref. 17 where the amount of alumina was small and instead the sample consisted of additional materials with lower emissivities; see discussion in ref. 18–20); the high emissivity was in fact validated experimentally in ref. 51. Accordingly, an energy balance for the top surface of the sample (similar to the one proposed in ref. 17) implied that the thermal emission is smaller but comparable with the heat conduction even at relatively weak illumination levels. Interestingly, the effective thermal conductivity of the sample reported in ref. 51, as extracted from the measurements, is indeed comparable with the thermal conductivities of gases, in accordance with the analysis of section 2. More specifically, it is easy to see that the extracted effective thermal conductivity of the sample reveals an increase with temperature, thus validating the main result of this work (see details in ESI section S5†).

Having said all the above, it is worth mentioning that a more careful modeling is needed for a better quantification of the effects of the thermal emission and the temperature-dependent thermal conductivity on the photothermal nonlinearity. Specifically, in addition to the radiative heat transfer between the catalyst sample and the chamber walls, one needs to account for the (unknown) temperature dependence of the

** Only limited data are available, *e.g.*, in ref. 69, only the imaginary part of the permittivity for photon energy 1.8–6 eV at 5 different temperatures (77, 295, 575, 770 and 920 K) is provided; in ref. 70, the permittivity data are provided at only 3 different temperatures (78, 293 and 423 K).

host emissivity and the temperature nonuniformities, emission from the bulk and its re-absorption *etc*. Nevertheless, from the examples analyzed above we can conclude that thermal emission may be playing a non-negligible role in the nonlinear photothermal response for temperatures of many hundreds of degrees and/or for high-emissivity systems.

6. Discussion

The analysis presented above was based on the initial modeling of the low-temperature response. Once the unknown system parameters were determined by fitting to the experimental data, the nonlinear photothermal response observed experimentally was modeled accurately using the known temperature dependence of the various material constituents, *i.e.*, using no additional fit parameters. The success of the photothermal analysis shows that as qualitatively predicted in section 2, the nonlinear response in the temperature rise originates primarily from the temperature dependence of the (effective) thermal conductivity of the host, and not from the response of the metal itself, nor the oxide support. We also identified the conditions under which thermal emission plays a non-negligible role.

This result shows that claims that the thermal model leads to unrealistic high temperatures are simply incorrect; see discussion in ref. 19. The metal nonlinearity could be of significance only for very thin plasmonic catalysts or even at the single nanoparticle level (see discussion in ref. 37–39). These systems are, however, usually of more fundamental rather than practical importance.

Unlike the generally weak effect of "hot" electrons, the photothermal nonlinearity is very strong. Therefore, this effect must be quantified before any claim for "hot" electron action can become convincing, and should not be ignored even at low illumination intensities. In practice, the rather large uncertainty in the magnitude of the associated nonlinear response coefficients means that only "hot" electron effects which are clearly greater than this uncertainty can be deduced. Unfortunately, satisfying these conditions poses a severe constraint on claims for "hot" electron dominance.

While the effect of the rising temperature on the absorptivity of the metal NPs may have a negligible effect on the overall temperature distribution, it may have a significant effect on the thermal emissivity *via* the Kirchhoff Law of Radiation, an effect already demonstrated experimentally.[72] This is relevant for the correct determination of the temperature using thermal imaging at mid-IR frequencies, *i.e.*, the change in emissivity at those frequencies would need to be accounted for at high temperatures. To the best of our knowledge, this has not been done so far in the context of plasmon-assisted photocatalysis; see the discussion in ref. 21.

At the high temperatures at which significant photothermal nonlinearity may be observed, the NPs themselves may undergo geometrical and morphological changes and eventually may even melt (at a temperature which may be significantly lower than the bulk melting temperature). This possibility was discussed in great detail in ref. 66 p. 270 ff. Briefly, while this effect may be possible, it was not probed directly, and it is *a-priori* expected not to affect the temperature distribution very much, especially not when $\delta_{skin} \ll H$.[31,51] Therefore, although melting may occur, it does not affect the results discussed in the current work in a significant manner.

Lastly, we note that systems similar to those studied here were extensively studied in the past in the context of composites with a high thermo-optical nonlinearity (see *e.g.*, ref. 35 and 46–49) and in the context of various applications such as optical limiting[50] or tunable optical devices.[35,73] The main difference is that the particle density in those systems was typically much lower, such that some (even most) of the light was transmitted through the sample. In addition, the focus in these systems was on (nonlinear) changes in the optical response (permittivity, transmission *etc*.), rather than on the temperature rise (as above).

The thermal effects in these systems were usually ignored, and the optical response was typically interpreted using a temporally and spatially local response. In that sense, it would be intriguing to study the thermal response in such systems, to see if the (temporally and spatially nonlocal) thermal effects could explain some of the experimental observations, in particular, the strong dependence on the spatial[74–76] and temporal extent of the illumination[45,77,78] and on the host properties.[37–39,79] In these cases, changes to the host permittivity may be more important, because of macroscopic transmission changes and thermal lensing effects, which were the main motivation for these studies in the first place.

Author contributions

I. W. Un derived the formulation, performed the calculations, and wrote the paper. Y. D. performed the initial fits to the experimental data and together with Y. S. supervised the project and contributed to the writing of the paper.

Conflicts of interest

There are no conflicts to declare.

Acknowledgements

I. W. U. and Y. S. were supported by Israel Science Foundation (ISF) grant (340/2020) and by Lower Saxony – Israel cooperation grant no. 76251-99-7/20 (ZN 3637). The authors would like to thank J. Baraban for many insightful discussions.

References

1 A. Nitzan and L. E. Brus, *J. Chem. Phys.*, 1981, **75**, 2205.
2 C. J. Chen and R. M. Osgood, *Phys. Rev. Lett.*, 1983, **50**, 1705.

3 R. Jin, Y. Cao, C. A. Mirkin, K. L. Kelly, G. C. Schatz and J. G. Zheng, *Science*, 2001, **294**, 1901–1903.
4 M. Maillard, P. Huang and L. Brus, *Nano Lett.*, 2003, **3**, 1611–1615.
5 Y. Tian and T. Tatsuma, *J. Am. Chem. Soc.*, 2005, **127**, 7632.
6 K. Ueno, S. Juodkazis, T. Shibuya, Y. Yokota, V. Mizeikis, K. Sasaki and H. Misawa, *J. Am. Chem. Soc.*, 2008, **130**, 6928–6929.
7 Y. Tsuboi, R. Shimizu, T. Shoji and N. Kitamura, *J. Am. Chem. Soc.*, 2009, **131**, 12623–12627.
8 G. Volpe, M. Noack, S. S. Acímović, C. Reinhardt and R. Quidant, *Nano Lett.*, 2012, **12**, 4864–4868.
9 C. Clavero, *Nat. Photonics*, 2014, **8**, 95–103.
10 G. Baffou and R. Quidant, *Chem. Soc. Rev.*, 2014, **43**, 3898.
11 W. Li and J. Valentine, *Nanophotonics*, 2016, **6**, 177–191.
12 K. Chen and H. Wang, *Mol. Syst. Des. Eng.*, 2021, **6**, 250–280.
13 S. Linic, P. Christopher and D. Ingram, *Nat. Mater.*, 2011, **10**, 911–921.
14 S. Mukherjee, F. Libisch, N. Large, O. Neumann, L. V. Brown, J. Cheng, J. B. Lassiter, E. A. Carter, P. Nordlander and N. J. Halas, *Nano Lett.*, 2013, **13**, 240–247.
15 P. Christopher, H. Xin, A. Marimuthu and S. Linic, *Nat. Mater.*, 2012, **11**, 1044–1050.
16 S. Mukherjee, L. Zhou, A. Goodman, N. Large, C. Ayala-Orozco, Y. Zhang, P. Nordlander and N. J. Halas, *J. Am. Chem. Soc.*, 2014, **136**, 64–67.
17 L. Zhou, D. F. Swearer, C. Zhang, H. Robatjazi, H. Zhao, L. Henderson, L. Dong, P. Christopher, E. A. Carter, P. Nordlander and N. J. Halas, *Science*, 2018, **362**, 69.
18 Y. Sivan, J. Baraban, I. W. Un and Y. Dubi, *Science*, 2019, **364**, eaaw9367.
19 Y. Sivan, J. Baraban and Y. Dubi, *OSA Continuum*, 2020, **3**, 483–497.
20 Y. Sivan, I. W. Un and Y. Dubi, *Chem. Sci.*, 2020, **11**, 5017–5027.
21 G. Baffou, I. Bordacchini, A. Baldi and R. Quidant, *Light: Sci. Appl.*, 2020, **9**, 108.
22 Y. Dubi, I. W. Un, J. Baraban and Y. Sivan, *Nat. Catal.*, 2022, in Print.
23 Y. Sivan and Y. Dubi, *Appl. Phys. Lett.*, 2020, **117**, 130501.
24 Y. Dubi and Y. Sivan, *Light: Sci. Appl.*, 2019, **8**, 89.
25 Y. Sivan, I. W. Un and Y. Dubi, *Faraday Discuss.*, 2019, **214**, 215–233.
26 R. Kamarudheen, G. W. Castellanos, L. P. J. Kamp, H. J. H. Clercx and A. Baldi, *ACS Nano*, 2018, **12**, 8447–8455.
27 X. Xu, A. Dutta, J. Khurgin, A. Wei, V. M. Shalaev and A. Boltasseva, *Laser Photonics Rev.*, 2020, **14**, 1900376.
28 S. Yu and P. K. Jain, *Nat. Commun.*, 2019, **10**, 2022.
29 X. Dai, Q. Wei, T. Duong and Y. Sun, *ChemNanoMat*, 2019, **5**, 1000–1007.
30 R. Kamarudheen, G. Kumari and A. Baldi, *Nat. Commun.*, 2020, **11**, 3957.
31 I. W. Un and Y. Sivan, *Nanoscale*, 2020, **12**, 17821–17832.
32 I. W. Un and Y. Sivan, *ACS Photonics*, 2021, **8**, 1183–1190.
33 X. Li, H. O. Everitt and J. Liu, *Nano Res.*, 2019, **19**, 1706–1711.
34 E. Pensa, J. Gargiulo, A. Lauri, S. Schlücker, E. Cortés and S. A. Maier, *Nano Lett.*, 2019, **19**, 1867–1874.
35 J. S. Donner, J. Morales-Dalmau, I. Aldaa, R. Marty and R. Quidant, *ACS Photonics*, 2015, **2**, 355–360.
36 S.-W. Chu, T.-Y. Su, R. Oketani, Y.-T. Huang, H.-Y. Wu, Y. Yonemaru, M. Yamanaka, H. Lee, G.-Y. Zhuo, M.-Y. Lee, S. Kawata and K. Fujita, *Phys. Rev. Lett.*, 2014, **112**, 017402.
37 Y. Sivan and S.-W. Chu, *Nanophotonics*, 2017, **6**, 317–328.
38 I. Gurwich and Y. Sivan, *Phys. Rev. E*, 2017, **96**, 012212.
39 I. W. Un and Y. Sivan, *Phys. Rev. Mater.*, 2020, **4**, 105201.
40 R. B. Wilson, B. A. Apgar, L. W. Martin and D. G. Cahill, *Opt. Express*, 2012, **20**, 28829–28838.
41 H. Reddy, U. Guler, K. Chaudhuri, A. Dutta, A. V. Kildishev, V. M. Shalaev and A. Boltasseva, *ACS Photonics*, 2017, **4**, 1083–1091.
42 H. Reddy, U. Guler, A. V. Kildishev, A. Boltasseva and V. M. Shalaev, *Opt. Mater. Express*, 2016, **6**, 2776–2802.
43 P.-T. Shen, Y. Sivan, C.-W. Lin, H.-L. Liu, C.-W. Chang and S.-W. Chu, *Opt. Express*, 2016, **24**, 19254.
44 Y. Osaka, S. Sugano and S. Hashimoto, *Nanoscale*, 2016, **8**, 18187–18196.
45 T. Stoll, P. Maioli, A. Crut, N. D. Fatti and F. Vallée, *Eur. Phys. J. B*, 2014, **87**, 260.
46 D. D. Smith, G. Fischer, R. W. Boyd and D. A. Gregory, *J. Opt. Soc. Am. B*, 1997, **14**, 1625.
47 R. W. Boyd, Z. Shi and I. D. Leon, *Opt. Commun.*, 2014, **326**, 74–79.
48 M. Rashidi-Huyeh and B. Palpant, *Phys. Rev. B: Condens. Matter Mater. Phys.*, 2006, **74**, 075405.
49 J. B. Khurgin and G. Sun, *Opt. Express*, 2013, **21**, 27460–27480.
50 J. Wang and W. J. Blau, *J. Opt. A: Pure Appl. Opt.*, 2009, **11**, 024001.
51 M. Xu, T. den Hartog, L. Cheng, M. Wolfs, R. Habets, J. Rohlfs, J. van den Ham, N. Meulendijks, F. Sastre and P. Buskens, *ChemPhotoChem*, 2022, e202100289.
52 P. Winsemius, M. Guerrisi and R. Rosei, *Phys. Rev. B: Solid State*, 1975, **12**, 4570–4572.
53 P. Winsemius, F. F. van Kampen, H. P. Lengkeek and C. G. van Went, *J. Phys. F: Met. Phys.*, 1976, **12**, 1583.
54 A. V. Gusarov and E. P. Kovalev, *Phys. Rev. B: Condens. Matter Mater. Phys.*, 2009, **80**, 024202.
55 R. B. Bird, W. E. Stewart and E. N. Lightfoot, *Transport Phenomena*, 2nd edn, 2002.
56 K. Pietrak and T. S. Wísniewski, *J. Power Technol.*, 2014, **95**, 14–24.
57 X. Li, X. Zhang, H. O. Everitt and J. Liu, *Nano Lett.*, 2019, **19**, 1706–1711.
58 Engineering ToolBox, *Nitrogen – Thermal Conductivity*, 2018.
59 Engineering ToolBox, *Hydrogen – Thermal Conductivity*, 2018.
60 S. C. Saxena and S. H. P. Chen, *Mol. Phys.*, 1975, **29**, 1507–1519.

61 S. Adachi, *The Handbook on Optical Constants of Metals*, World Scientific, 2012.
62 X. Zhang, X. Li, M. E. Reish, D. Zhang, N. Q. Su, Y. Gutiërrez, F. Moreno, W. Yang, H. O. Everitt and J. Liu, *Nano Lett.*, 2018, **18**, 1714–1723.
63 Engineering ToolBox, *Carbon dioxide – Thermal Conductivity*, 2018.
64 R. Afshar, S. Murad and S. C. Saxena, *Chem. Eng. Commun.*, 1981, **10**, 1–11.
65 Engineering ToolBox, *Ammonia – Thermal Conductivity at Varying Temperature and Pressure*, 2018.
66 J. Aizpurua, F. Baletto, J. Baumberg, P. Christopher, B. d. Nijs, P. Deshpande, Y. Diaz Fernandez, L. Fabris, S. Freakley, S. Gawinkowski, A. Govorov, N. Halas, R. Hernandez, B. Jankiewicz, J. Khurgin, M. Kuisma, P. V. Kumar, J. Lischner, J. Liu, A. Marini, R. J. Maurer, N. S. Mueller, M. Parente, J. Y. Park, S. Reich, Y. Sivan, G. Tagliabue, L. Torrente-Murciano, M. Thangamuthu, X. Xiao and A. Zayats, *Faraday Discuss.*, 2019, **214**, 245–281.
67 F. W. Sears and G. L. Salinger, *Thermodynamics, kinetic theory, and statistical thermodynamics*, Addison-Wesley, Boston, MA, 3rd edn, 1975.
68 A. M. Hofmeister, *Phys. Chem. Miner.*, 2014, **41**, 361–371.
69 G. Pells and M. Shiga, *J. Phys. C: Solid State Phys.*, 1969, **2**, 1835.
70 P. B. Johnson and R. W. Christy, *Phys. Rev. B: Solid State*, 1975, **11**, 1315–1323.
71 Mikron Instrument Company, Inc., *Table of Emissivity of Various Surfaces for Infrared Thermometry*, 2018.
72 T. E. Ariceta, PhD Thesis, 2016.
73 J. S. Donner, G. Baffou, D. McCloskey and R. Quidant, *ACS Nano*, 2011, **5**, 5457–5462.
74 A. A. Maznev, J. A. Johnson and K. A. Nelson, *J. Appl. Phys.*, 2011, **109**, 073517.
75 A. Block, M. Liebel, R. Yu, M. Spector, Y. Sivan, J. G. de Abajo and N. F. van Hulst, *Sci. Adv.*, 2019, **5**, eaav8965.
76 Y. Sivan and M. Spector, *ACS Photonics*, 2020, **7**, 1271–1279.
77 F. Masia, W. Langbein and P. Borri, *Phys. Rev. B: Condens. Matter Mater. Phys.*, 2012, **85**, 235403.
78 A. Marini, M. Conforti, G. D. Valle, H. W. Lee, T. X. Tran, W. Chang, M. A. Schmidt, S. Longhi, P. S. J. Russell and F. Biancalana, *New J. Phys.*, 2013, **15**, 013033.
79 G. Baffou, R. Quidant and F. J. G. de Abajo, *ACS Nano*, 2010, **4**, 709–716.